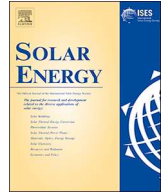




ELSEVIER

Contents lists available at ScienceDirect

Solar Energy

journal homepage: www.elsevier.com/locate/solener

A co-located solar receiver and thermal storage concept using silicate glass at 1000 °C and above: Experiments and modeling in the optically-thick regime

E. Casati^{a,b,*}, A. Lankhorst^c, U. Desideri^b, A. Steinfeld^a

^a Department of Mechanical and Process Engineering, ETH Zurich, Sonneggstrasse 3, CH-8092 Zurich, Switzerland

^b Department DESTEC, University of Pisa, Largo L. Lazzarino, 56122 Pisa, Italy

^c CelSian Glass & Solar BV, Zwaanstraat 1, 5651 CA Eindhoven, The Netherlands

ARTICLE INFO

Keywords:

Concentrating Solar Power (CSP)

Thermal Energy Storage (TES)

Glass

GLASUNTES

ABSTRACT

This work presents the exploratory experimental results of a co-located solar receiver and thermal energy storage (TES) concept based on a pool of molten glass contained in a cavity, serving as solar receiver and TES medium simultaneously. Distinctive features of the system are the direct and volumetric absorption of solar radiation by the semi-transparent glass and a stationary TES medium. Only the charge cycle was studied, without a heat-removal system. Recycled soda-lime-silica (SLS) container glass of various colors was adopted as working medium in a setup tested at the ETH's High Flux Solar Simulator (HFSS). A steady 3D heat transfer model of the experimental apparatus, which couples Monte-Carlo ray-tracing and CFD techniques, was developed and validated against the experimental results. The tests used the HFSS as the only energy source, with maximum radiative fluxes of 1.2 MW m^{-2} and power input of 1.5 kW directly absorbed by the glass, which reached measured temperatures of 1300 °C , while the maximum temperatures –as predicted by the model– exceeded 1500 °C . Such conditions were maintained for 5 to 10 h and no technical problems were encountered with the containment of the hot glass melt. These preliminary results demonstrate that silicate glasses are effective volumetric absorbers of solar radiation up to temperatures exceeding 1300 °C .

1. Introduction

Concentrated solar power (CSP) uses highly concentrating optics to deliver heat at temperatures exceeding 2000 °C , allowing to drive high temperature industrial processes. Notable examples are the production of electricity (Jelley and Smith, 2015), carbon-neutral fuels (Romero and Steinfeld, 2012) and the metallurgical extraction processes (Steinfeld, 1997; Davis et al., 2017). When integrated with thermal energy storage (TES) systems, these power generation and thermochemical processes can be operated continuously and round-the-clock, despite the intermittent nature of solar irradiation.

To exploit this potential, further developments of TES systems are needed for operating at 1000 °C and above. Current state-of-the-art is based on molten salts at approximately 565 °C . Higher temperatures call for new salt formulations, each bringing new challenges as the corrosion mechanisms differ among candidate salts (Mehos et al., 2017). A number of works review the status and the latest advancements in the field of high temperature TES, e.g., Kuravi et al. (2013), Prieto et al.

(2016), Zhang et al. (2016) and Pelay et al. (2017).

Due to their favorable properties in terms of high temperature resistance and compatibility with other materials, molten glasses are receiving attention as candidate TES materials. Glass is a non-crystalline amorphous solid made of refractory oxides such as silica (SiO_2), lime (Ca(OH)_2) and soda (Na_2CO_3). These are among the most abundant elements on earth's crust, evenly distributed and inexpensive. The manufacture of glass is an ancient industry, where temperatures of the order of 1600 °C are routinely dealt with for centuries (Cable, 2006). Extensive knowledge of the processes involved is available (Kraus and Horst, 2002) and solutions to technological issues such as the glass melt containment are established industrially (Bingham et al., 2011; Selkregg, 2018).

Elkin et al. (2013) proposed to substitute molten salts with oxide glasses as the heat transfer fluids (HTFs) and TES media in CSP plants based on the two-tank sensible-heat storage concept (Kuravi et al., 2013). This requires the glass to be circulated to a heat exchanger and a tower-mounted solar receiver which, due to the very high viscosities, is

* Corresponding author at: Department of Mechanical and Process Engineering, ETH Zurich, Sonneggstrasse 3, CH-8092 Zurich, Switzerland.

E-mail address: casatie@ethz.ch (E. Casati).

<https://doi.org/10.1016/j.solener.2018.11.052>

Received 14 August 2018; Received in revised form 7 November 2018; Accepted 20 November 2018

0038-092X/ © 2018 Published by Elsevier Ltd.

Nomenclature

Symbols

Q_{conv}	convective heat losses from external walls (W)
h_{conv}	convective heat transfer coefficient ($\text{Wm}^{-2}\text{K}^{-1}$)
T_{∞}	surroundings temperature (K)
$Q_{\text{rad,walls}}$	radiative heat losses from external walls (W)
$Q_{\text{rad,ap}}$	radiative heat losses from aperture (W)
T_{ap}	aperture temperature (K)
S_{solar}	radiative source term in Eq. (2) (Wm^{-3})
T	temperature (K or °C)
E_{λ}	spectral emissive power ($\text{Wm}^{-2}\mu\text{m}^{-1}$)
$I_{\text{b}\lambda}$	blackbody spectral radiative intensity ($\text{Wm}^{-2}\mu\text{m}^{-1}$)
T_{S}	source temperature in Eq. (1) (K)
l_{m}	Planck-mean photon mean-path length (mm)
L	characteristic system length (mm)
\mathbf{q}_{c}	conductive heat flux vector (Wm^{-2})
\mathbf{q}_{r}	radiative heat flux vector (Wm^{-2})
k	molecular thermal conductivity ($\text{Wm}^{-1}\text{K}^{-1}$)
n	refractive index
κ_{R}	radiative conductivity ($\text{Wm}^{-1}\text{K}^{-1}$), Eqs. (6) and (9)
k_{eff}	glass effective thermal conductivity ($\text{Wm}^{-1}\text{K}^{-1}$)

Greek Symbols

ϵ_{walls}	external walls emittance
ϵ_{ap}	aperture emittance
λ	wavelength (μm)
κ_{λ}	spectral absorption coefficient (cm^{-1})
κ_{m}	Planck-mean absorption coefficient (cm^{-1}), Eq. (1)
τ_{L}	optical thickness
σ	Stefan–Boltzmann constant ($\text{Wm}^{-2}\text{K}^{-4}$)
κ_{R}	Rosseland-mean absorption coefficient (cm^{-1}), Eq. (5)

Abbreviations

CSP	concentrated solar power
TES	thermal energy storage
HTF	heat transfer fluid
SLS	soda-lime-silica
EU	European Union
MCRT	Monte Carlo ray-tracing
CFD	computational fluid dynamics
TC	thermocouple
ETH	Swiss federal institute of technology - Zurich
HFSS	high flux solar simulator
CCD	charge-coupled device

impractical for common glasses. New phosphorous glass formulations are proposed for the range 400–1200 °C (Elkin et al., 2013), to be used in a solar receiver based on a directly-irradiated 2–3 mm thick falling glass film (Herrera et al., 2017). Cárdenas et al. (2016) proposed a different TES concept where molten container glass is indirectly heated to 1000 °C through an upward-facing cavity receiver. Graphite insertions are used to enhance the energy transfer to the container bottom, where the heat extraction process takes place. These previous studies do not present experimental results. Other authors are investigating the use of glasses as phase change materials, and encouraging experimental evidences have already been reported for low temperature applications (Muramoto et al., 2018).

In the framework of the EU-funded project GLASUNTES¹, a co-located solar receiver and TES concept is investigated. It consists of a molten glass pool contained in a cavity, serving as solar receiver and TES medium simultaneously. Similar systems have been proposed, mainly for the use with molten salts (Epstein et al., 1999; Slocum et al., 2011; Badenhorst et al., 2016). In particular, the CSPonD concept introduced by Slocum et al. (2011) is currently in the demonstration phase (Gil et al., 2015; Gil et al., 2017).

Distinctive features of the system are the direct and volumetric absorption of solar radiation by the semi-transparent glass melt and a stationary TES medium. In this work, we describe the first experimental results for the charge cycle (without a heat-removal system), using recycled soda-lime-silica (SLS) container glass of various colors. We discuss a steady 3D heat transfer model to simulate the experimental apparatus. The model couples Monte Carlo ray-tracing (MCRT) and Computational Fluid Dynamics (CFD) techniques and is validated by comparing numerically calculated and experimentally measured temperatures of the glass melt. This validated simulation model can serve as a tool for the further development of this technology, notably, the design and optimization of a scale-up demonstration system.

The work is structured as follows. The experimental setup is described in Section 2. The process of radiative heat transfer in hot glass is discussed in Section 3 and the developed model is introduced in Section 4. The experimental results are presented in Section 5, while the conclusions and an outlook to future work in Section 6.

2. System configuration and experimental setup

A schematic of the experimental setup is shown in Fig. 1(a). Fig. 1(b) shows the photograph of the setup during experiments. An alumina crucible is placed inside a shell made by Al_2O_3 - SiO_2 fibrous insulation boards. A board of the same material serves as the lid of the cavity. A tapered circular aperture with 40 mm diameter is machined in this lid, allowing for the access of concentrated solar radiation into the cavity from the top, according to the beam-down optical configuration (Rabl, 1976; Segal and Epstein, 1999).² A maximum of 4.5 kg of pulverized glass can be loaded in the crucible, resulting in a melt height of about 55 mm. The main sizes of the setup are reported in Fig. 2.

2.1. Glass samples

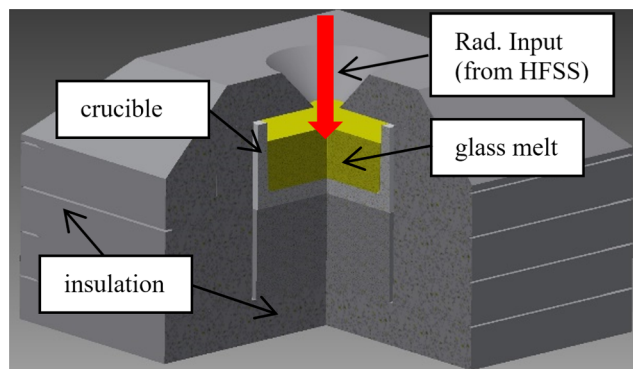
Several samples of amber and clear SLS container glass were used in the tests. The glass came from a recycling plant in the form of cullet, which was rinsed with water, dried, and then pulverized to a final size of approximately 20 μm . The chemical composition, measured by X-ray diffraction, comprised 70.5 wt% SiO_2 , 12.4 wt% Na_2O , 10.3 wt% CaO , 2.5 wt% MgO , 2.1 wt% Al_2O_3 , and 1.2 wt% K_2O . This composition is common to all the samples and is well in line with standard SLS container glass formulations (Seward and Vascott, 2005). The amber glass used in this study has 0.38 wt% of iron as Fe_2O_3 and 0.034 wt% of chromium as Cr_2O_3 , while the clear glass has 0.05 wt% and 0.002 wt%, respectively. As detailed in the following, these trace components are added as coloring agents. The remainder is constituted by minor amounts of Ti, Mn, Pb and Zr oxides (0.6–0.7 wt% in total).

2.2. Temperature measurements

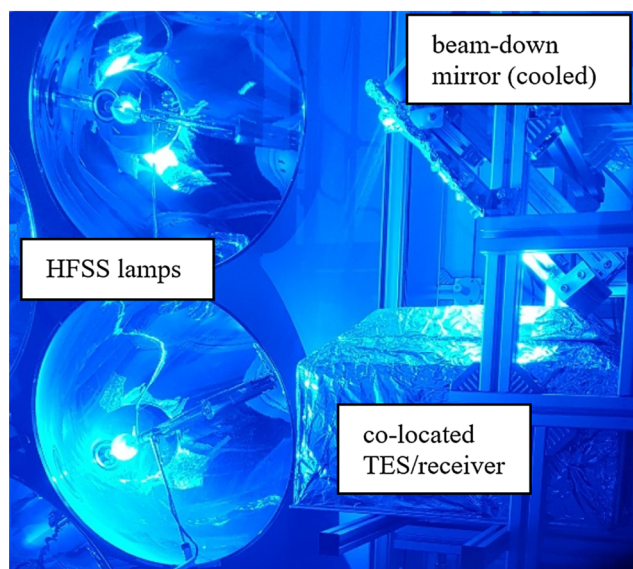
Measuring the temperature distribution of hot glass bodies is in general a difficult task because of errors introduced by internal radiative heat transfer (Glicksman and Renier, 1973). Thermocouples are commonly adopted due to their accuracy and simplicity (Viskanta et al., 1975, 1993, 2014) and, for the same reason, were selected in the present study.

¹ Project website: www.glasuntes.eu.

² Note that no secondary concentrator is used in this case.



(a)



(b)

Fig. 1. Schematic of the experimental setup (a), and photograph of the setup in the HFSS during testing (b).

A multi-point thermocouple probe was designed and built. Three standard S-type thermocouple-wires (90% Pt-10% Rh/Pt) with a diameter of 0.35 mm were inserted in a custom made ceramic assembly, obtained from 6-bore dense alumina tubes with external and bore diameter of 4 and 0.8 mm, respectively. The instrument thus assembled, shown in Fig. 3, allows to measure 3 temperatures. This is then inserted into a ceramic closed-end tube with 7 mm external diameter, with the aim of shielding the measurement joints from the radiation source, and to prevent the poisoning of the platinum-based wires by silica (Kinzie, 1973). The shield gets trapped in the glass upon cooling and solidification after each test, while the instrument can be extracted and reused. By inserting two such probes, a grid of 6 measuring points within the glass is obtained, as indicated by the legend TC 1 to TC 6 in Fig. 2. The measurement accuracy is within ± 5 °C at the maximum temperatures reached during the experiments.

Other S-type TCs are used to monitor the temperature of the crucible bottom (TC 8–9) and side (TC 7) walls, while K-type TCs are placed in the insulation shell (TC 10–12) and in the lid (TC 14–15). Additional TCs (not shown) were placed in the plane normal to Fig. 2 and containing the aperture axis, in positions corresponding to TC 7, 11 and 12.

2.3. The HFSS

Experimentation was performed at the ETH's High Flux Solar

Simulator (HFSS): an array of 7 Xenon short-arc lamps (Osram XBO 6000 W), each coupled to a truncated ellipsoidal reflector having a common focal point, see Petrasch et al. (2007).³ The HFSS provides a source of intense thermal radiation that approximates the heat transfer characteristics of highly concentrating solar systems, see Fig. 4(a).

The setup is positioned with the aperture located in the focal plane of the HFSS. In order to do so, the incoming beam is redirected downwards by a water-cooled 45° mirror and enters the setup from the top, as shown in Fig. 1. The radiative flux distribution at the focal plane point where the mirror intersects the beam was measured optically using a calibrated CCD camera focused on a water-cooled Al₂O₃-coated Lambertian target. The radiative power input was determined using a water-calorimeter. By design, the entering flux impinges on a central region of the melt surface, representing approximately 20% of the total exposed top surface.

2.4. Procedure

A typical experimental run lasted up to 10 h, and it consisted of two consecutive stages. During the first stage, the setup was heated from cold conditions using the HFSS as the sole energy source. The radiative power input was controlled such that the measured temperature non-uniformities over the crucible walls did not exceed 150 °C, nor the heating rate 300 °C min⁻¹, in order to prevent excess thermal stresses leading to failures of the crucible itself. The heating process continued as long as it was possible to fulfill these constraints, considering that the total experiment time could not exceed twelve hours.

The second stage aimed at reaching steady-state conditions: the power input was kept constant until the variations of all the measured temperatures dropped below ± 0.2 °C min⁻¹. The maximum power input was 1.5 kW for all the tests performed, corresponding to a mean solar concentration ratio over the aperture of approximately 1200 suns.⁴

2.5. Experimental results

For all the tests performed, it was possible to completely melt the glass powder loaded in the crucible, Fig. 5(a), to reach and maintain temperatures exceeding 1000 °C and to obtain a melt with depth around 55 mm.

In the case of clear glass, it was not possible to increase the melt temperature without overheating the crucible bottom. The maximum glass temperature achieved was thus limited to 1145 °C, and the obtained melt was rather heterogenous. Conversely, the heating process was easily controlled during the tests employing amber glass: measured melt temperatures around 1300 °C were reached and maintained for more than 5 h, and the melt obtained was very uniform, as shown in Fig. 5(b).

3. Radiative heat transfer in hot glass

As temperature increases above 500–600 °C, radiative exchange becomes the dominant heat transfer mechanism in homogeneous semi-transparent materials, which can be modeled as absorbing-emitting media (Viskanta and Anderson, 1975). The absorption coefficient of SLS glasses varies over more than three orders of magnitude in the range of wavelengths of interest for thermal systems. This can be seen in Fig. 4(b), showing the spectral absorption coefficient κ_λ of a clear and of an amber SLS container glass representative of the materials used in this study. To construct the figure, the data of Endrýs et al. (1997) have been complemented in the UV region considering the cutoff due to charge transfer phenomena, which makes SLS glasses opaque for

³ In the reference, a previous HFSS model developed by the research group is described, which has 11 lamps instead of 7.

⁴ Concentration ratio expressed in “suns”, i.e., normalized to 1 kW m⁻².

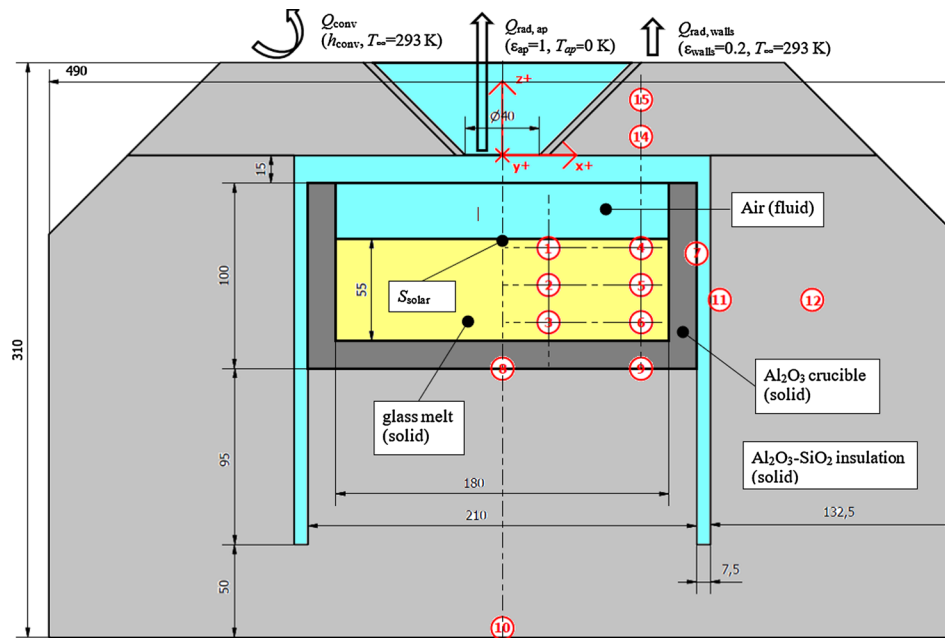


Fig. 2. Section-view of the co-located solar receiver-TES system model, showing the thermocouples positions, the modeling domains, the boundary conditions, and the source term (sizes in mm).

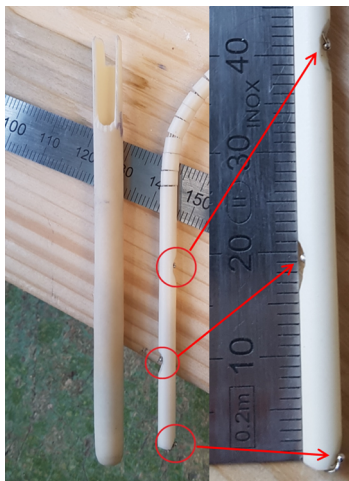


Fig. 3. Three points temperature probe. From the left: ceramic shield, probe with measuring joints marked by the red circles, and detail view. (For interpretation of the references to colour in this figure legend, the reader is referred to the web version of this article.)

wavelengths lower than approximately $0.34 \mu\text{m}$, irrespective of temperature and concentration of coloring agents (Ades et al., 1990). Other features common to SLS glasses are the increased infrared absorption due to vibration of the hydroxyl groupings starting around $2.8 \mu\text{m}$, and of the basic silica framework from approximately $4.2 \mu\text{m}$ (Ades et al., 1990; Choudhary and Potter, 2005). The major components of silicate glasses are weak absorbers in the $0.5 < \lambda < 2.5 \mu\text{m}$ region. On the other hand, trace materials like the first row transition metal ions can cause significant absorption of visible light, and are commonly added as coloring agents. In standard container glasses mainly iron and chromium ions are used, and both the intensity and the wavelength of absorption depend on their oxidation state and coordination, in turn influenced by melting conditions and temperature (Bamford, 1978).

Glasses containing only low amount of iron and chromium, and produced under oxidizing conditions (i.e., iron mostly present as Fe^{3+}), feature a comparatively low absorption in the $0.5 < \lambda < 2.5 \mu\text{m}$ region, as can be seen for the clear glass in Fig. 4(b). For glasses with relatively

high iron content and produced in reducing atmosphere, like amber glass, the absorption band of Fe^{2+} around $1.0\text{--}1.1 \mu\text{m}$ dominates the spectra between 0.5 and $2.5 \mu\text{m}$. In general, the absorption strength of the Fe^{2+} band in these glasses decreases with temperature (Faber, 2002; Choudhary and Potter, 2005), as shown in Fig. 4(b).

The Planck-mean absorption coefficient, defined as (Modest, 2013)

$$\kappa_m \equiv \frac{\int_0^\infty I_{b\lambda}(T_s) \kappa_\lambda(T) d\lambda}{\int_0^\infty I_{b\lambda}(T_s) d\lambda}, \quad (1)$$

can be adopted to evaluate the spectrally-averaged absorption of radiation from a source at temperature T_s by a medium at temperature T . In Eq. (1), $I_{b\lambda}$ is the blackbody spectral radiative intensity of the source and $T_s = 5777 \text{ K}$ is assumed for solar radiation. The values of κ_λ for the glass are taken from Endrýs et al. (1997) and linearly interpolated for intermediate temperature values. Variations of the redox state during the tests are neglected, given the very low diffusivity of atmospheric oxygen in the melt. Eq. (1) is solved by integrating numerically over the spectral window $0.3 < \lambda < 4.5 \mu\text{m}$, which contains 96% of the blackbody emission at 5777 K . The resulting κ_m values for the two glasses at different temperatures are listed in Table 1, together with the corresponding photon mean-path length $l_m = \kappa_m^{-1}$.

Hot glass is a medium participating in the radiative heat transfer, for which the optical thickness based on the extinction of radiation traveling in direction $\hat{\mathbf{i}}$ is $\tau_{\hat{\mathbf{i}}} = \int_0^L \kappa_m(l) dl$. Considering the average melt depth $L = 55 \text{ mm}$ as the characteristic system length, the optical thickness of the problem at hand is evaluated as $\tau_L = \kappa_m L$, assuming κ_m to be constant over L . Also the τ_L values are reported in Table 1.

4. Heat transfer model

A 3D heat transfer model was developed to simulate the experiments performed with the amber glass. The computational domains of the model – fluid and solid – are indicated in Fig. 2. The insulation and the crucible are modeled as solid domains. Being the cavity open, the air contained in it is heated during the experiments and flows through the aperture due to buoyancy. However, no bulk flow establishes through upward-facing apertures, but a slow and unstable streaming due to the impediment of the outflow from the cavity by the inflow, resulting in a reduction of convection losses with respect to, e.g.,

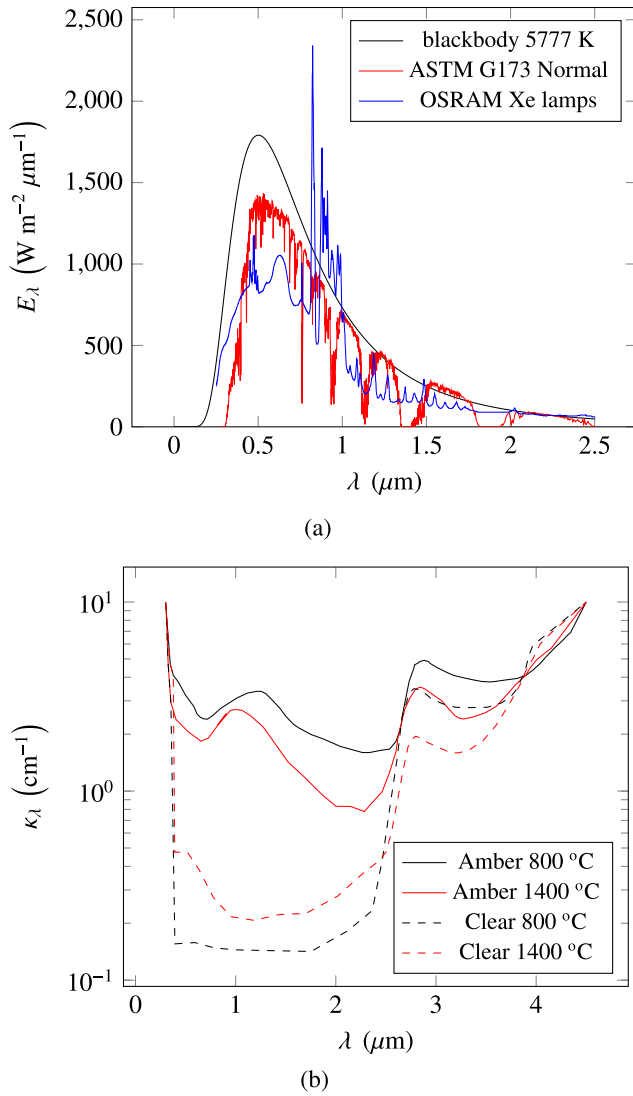


Fig. 4. (a) Emission spectra for a blackbody at 5777 K, for the terrestrial direct solar radiation according to the ASTM G-173-03 standard, and for the HFSS lamps. (b) Spectral absorption coefficient κ_λ for clear and amber container glass at 800 °C and 1400 °C, adapted from [Endrýs et al. \(1997\)](#).

horizontal apertures ([Taumoefolau et al., 2004](#); [Leibfried and Ortjohann, 1995](#)). Heat losses due to natural convection of ambient air in the cavity are therefore neglected in the present analysis, and air is treated as a stagnant fluid not participating in the radiative transfer.

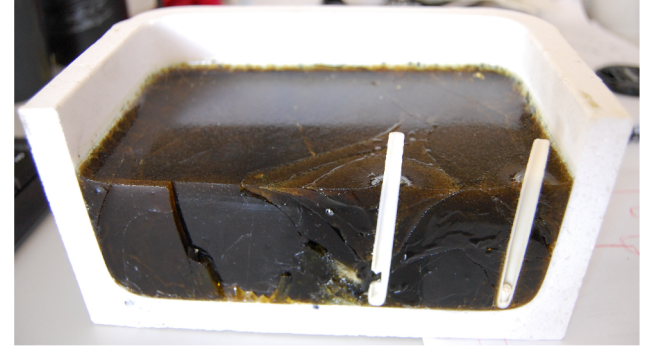
Significant natural convection currents are not expected to establish in the glass melt either, mainly due to its high viscosity (40 Pa·s at 1300 °C) and small depth. For the experiments with the highest measured glass temperatures, the Rayleigh number is approximately 250, while the critical value for the inception of convection in glass melts is around 1700 ([Eryou and Glicksman, 1972](#)). Therefore, natural convection in the glass melt is considered negligible with respect to the predominant radiative transfer mode and the melt itself is modeled as a participating solid body. Notably, the melting process is not modeled since this occurs at temperatures around 600 °C, which are far lower than the temperature levels of interest in the present study, i.e., above 1000 °C.

4.1. Governing equations

In the absence of motion, the energy conservation equation alone suffices to model the system, i.e., in steady vector form ([Modest, 2013](#)),



(a)



(b)

Fig. 5. (a) Amber glass powder loaded in the crucible before testing, and (b) glass block obtained after cooling (section cut along the mid-plane, including the thermocouples shields).

Table 1

Planck-mean absorption coefficient κ_m of container glasses irradiated by a blackbody source at $T_S = 5777$ K (Eq. (1)), corresponding photon mean-path length $l_m = \kappa_m^{-1}$, optical thickness $\bar{\tau}_l$ for a melt depth of 55 mm, and Rosseland-mean absorption coefficient κ_R (Eq. (5)).

Glass	T (°C)	κ_m (cm^{-1})	l_m (mm)	$\bar{\tau}_l=55\text{mm}$	κ_R (cm^{-1})
Amber	800	3.15	3.2	17.2	3.37
	1000	2.86	3.5	15.7	2.55
	1200	2.60	3.8	14.5	2.02
	1400	2.35	4.2	13.1	1.60
Clear	800	0.52	19.0	2.9	
	1000	0.64	15.6	3.5	
	1200	0.71	14.1	3.9	
	1400	0.80	12.5	4.4	

$$S_{\text{solar}} - \nabla \cdot \mathbf{q}_c - \nabla \cdot \mathbf{q}_r = 0. \quad (2)$$

In Eq. (2), $\nabla \cdot \mathbf{q}_c$ and $\nabla \cdot \mathbf{q}_r$ are the divergence of the conductive and radiative heat flux vectors, respectively, and S_{solar} is the source term accounting for the incoming solar radiation from the HFSS.

The conduction transfers are modeled according to the Fourier's formulation of heat diffusion

$$\mathbf{q}_c = -k \nabla T, \quad (3)$$

where k is the phonon (or molecular) thermal conductivity of the given material. The radiative heat transfer within the cavity is modeled following the radiosity method ([Modest, 2013](#)), considering the insulation and crucible walls as opaque and diffusely reflecting surfaces, the melt surface as specularly reflecting, and modeling the aperture as a black surface at 0 K.

When $\bar{\tau}_l$ is much larger than unity, as it is the case for the amber

Table 2
Material properties used in the CFD analysis.

		T (K)	Ref.
Al₂O₃-SiO₂ insulation			
Th. conductivity (W m ⁻¹ K ⁻¹)	1.741 e- 1 - 2.452 e- 4·T + 3.067 e- 7·T ²	600–1200	Kapyfract (2016)
Hemispherical total emittance	0.3	-	Touloukian and Dewitt (1972)
Crucible (porous alumina 97%)			
Th. conductivity (W m ⁻¹ K ⁻¹)	2.5	300	Almath Crucibles (2018)
Hemispherical total emittance	0.3	-	Touloukian and Dewitt (1972)
Glass (amber)			
Th. conductivity (W m ⁻¹ K ⁻¹)	1	300–1773	Seward and Vascott (2005)
Rad. conductivity (W m ⁻¹ K ⁻¹)	See Eq. (9)	873–1673	Endrýs et al. (1997)
Surface emittance	0.9	-	Lee and Viskanta (2001)
Air			
Th. conductivity (mW m ⁻¹ K ⁻¹)	0.11e1 + 8.79 e- 2·T - 2.17 e- 5·T ²	60–2000	Stephan and Laesecke (1985)

glass (Table 1), the medium can be considered *optically thick* and the radiative heat flux can be expressed as (Modest, 2013)

$$\mathbf{q}_r = -\frac{4\sigma}{3\kappa_R} \frac{d(n^2T^4)}{dl}, \quad (4)$$

where κ_R is the *Rosseland-mean extinction coefficient* defined as

$$\frac{1}{\kappa_R} \equiv \frac{\pi}{4\sigma T^3} \int_0^\infty \frac{1}{\kappa_\lambda} \frac{dl_{b\lambda}}{dT} d\lambda. \quad (5)$$

Eqs. (4) and (5) express the well known Rosseland approximation (Rosseland, 1936), which leads to define a *radiative conductivity* k_R as

$$k_R = \frac{16n^2\sigma T^3}{3\kappa_R}. \quad (6)$$

This approach allows to reduce the radiation problem in the glass to a heat-diffusion process with strongly temperature-dependent conductivity, i.e. (Modest, 2013),

$$\mathbf{q}_r = -k_R \nabla T|_{\text{glass}}. \quad (7)$$

In the optically-thick case, the conductive and radiative source terms in Eq. (2) can thus be expressed, for the glass, as

$$-\nabla \cdot \mathbf{q}_c - \nabla \cdot \mathbf{q}_r = \nabla \cdot (k_{\text{eff}} \nabla T)|_{\text{glass}}, \quad (8)$$

where k_{eff} is the glass *effective thermal conductivity* $k_{\text{eff}} = k_R + k$.

Eq. (6) is solved integrating numerically over the spectral window $0.3 < \lambda < 4.5 \mu\text{m}$ using the data of Endrýs et al. (1997) for the amber glass. This range of wavelengths contains all the significant contributions to the radiative heat transfer in SLS glasses at these temperatures, as detailed by Choudhary and Potter (2005). Discrete κ_R values thus calculated are reported in Table 1. The k_R results in the 800 – 1400 °C can be fitted with a third-degree polynomial as

$$k_R = -3.930e1 + 1.068 e- 1 \cdot T - 9.891 e- 5 \cdot T^2 + 3.375e \cdot T^3, \quad (9)$$

where the temperature is in degrees Kelvin.

Notably, the diffusion approximation should be adopted with caution since, as the optical thickness gets smaller and closer to unity – and/or close to the container walls – the concept of radiative conductivity itself ceases to be well defined and the predictions obtained with this method loose accuracy and physical meaning (Modest, 2013; Viskanta and Song, 1985).

4.2. Material properties

Material properties used in the CFD modeling are listed in Table 2. The thermal conductivity and the optical properties of the Al₂O₃-SiO₂ insulation and of the crucible were taken from the manufacturers and from the literature (Touloukian and Dewitt, 1972).

4.3. Boundary conditions and source term

The boundary conditions and source term are schematically indicated in Fig. 2. The radiative power input delivered by the HFSS and absorbed within the cavity-receiver was determined by MCRT, yielding the energy source S_{solar} to the CFD code, where it is assumed to be absorbed on the glass surface. At the outer walls, natural convective heat transfer is modeled using Nusselt correlations for flat surfaces such as those proposed by Churchill and Chu (1975). Given the comparatively large thickness of the insulation, the problem is dominated by heat-diffusion. Therefore, inaccuracies in the estimation of the outer convective heat transfer have a negligible influence on the results. Radiative heat losses from the walls are calculated assuming black surroundings at temperature $T_\infty = 293$ K and $\epsilon_{\text{walls}} = 0.2$.

4.4. Numerical solution

The MCRT simulations of S_{solar} were performed using the in-house code VEGAS (Petrasch, 2010). The CFD simulations were performed with ANSYS Fluent 18.2, and the available radiosity method implementation – called *surface to surface* model – was used to solve the radiative heat transfer within the cavity. The key input for the method, i.e., the view factors between the cavity walls, were also calculated by MCRT using VEGAS. The governing equation is discretized in space (approximately 250,000 cells, mixed parallelepipeds and tetrahedrons) and solved on all the cells by the finite-volume method with a third-order accurate scheme (ANSYS, 2018; van Leer, 1979).

5. Experimental validation and results

The MCRT simulation of the HFSS was experimentally validated with measurements of the radiative flux distribution at the mirror plane, as detailed in Furler and Steinfeld (2015). The radiative power input through the aperture of the co-located receiver-TES model was obtained by integration of the simulated flux, and verified against measurements using a water-calorimeter. Note that the concentrated beam expands after entering the cavity through its aperture. The simulated distribution of the heat flux absorbed on the glass surface is shown in Fig. 6(a).

Experimental validation of the heat transfer model was accomplished by comparing its numerical output to the experimental measurements. The calculated temperature field in the glass is shown in Fig. 6(b), and Table 3 reports the comparison with the measured values. The agreement is in general satisfactory, particularly for the locations farther from the walls. Discrepancies are attributed to the intrinsic limitations of the diffusion approximation adopted to model the radiative transfer within the melt, to inaccuracies in the high temperature

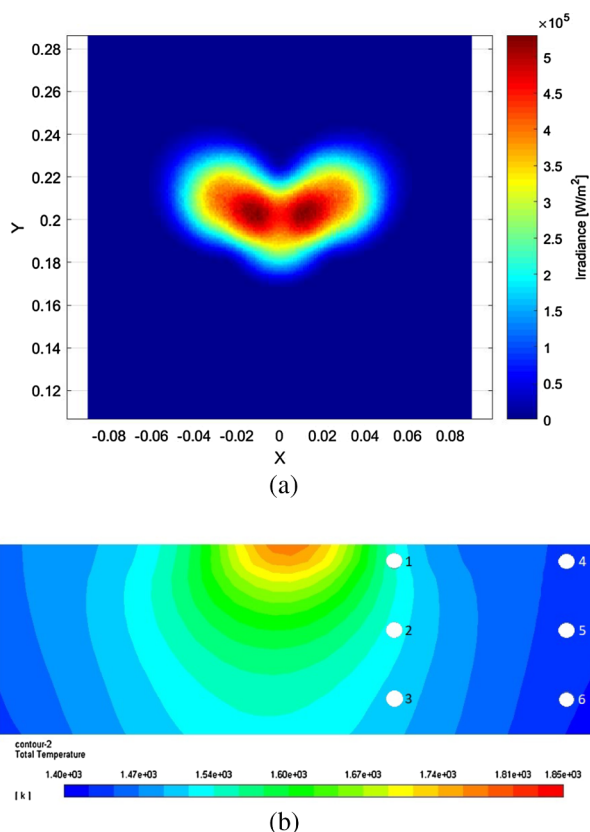


Fig. 6. (a) Simulated radiative flux distribution on the glass surface. (b) temperature field in the glass mid plane (X-Z plane, see Fig. 2), the white dots represent the thermocouples.

Table 3

Experimentally measured vs. calculated temperatures in the glass. See Fig. 6(b) for thermocouples positions.

TC No.	T_{exp} (°C)	T_{calc} (°C)	$(T_{exp} - T_{calc})/T_{exp}$ %
1	1278	1266	-1.0
2	1248	1251	0.2
3	1217	1229	1.0
4	1150	1168	1.6
5	1131	1162	2.7
6	1119	1154	3.1

material properties (most notably for the Al_2O_3 - SiO_2 insulation) and to uncertainties in the positioning of the thermocouples.

It can be seen that the predicted temperatures in the glass region where the HFSS flux is initially absorbed reach maximum values exceeding 1500 °C. This was qualitative verified during the experiments, where a corresponding region of lower-viscosity melt was observed with a CCD camera looking through the aperture.

6. Conclusions and outlook

This work presents the exploratory experimental results of a co-located solar receiver and TES concept based on a pool of molten glass contained in a cavity, serving as solar receiver and TES medium simultaneously. Only the charge cycle was studied, without a heat-removal system. Recycled soda-lime-silica (SLS) container glass of various colors was adopted as working medium in a setup built and tested at the ETH's High Flux Solar Simulator (HFSS). A steady 3D heat transfer model of the experimental apparatus, which couples Monte-Carlo ray-tracing and CFD techniques, was developed and validated against the experimental results. This simulation tool can support following

development steps of the proposed concept.

The tests started from cold conditions and used the HFSS as the sole energy source, with maximum fluxes of 1.2 MW m^{-2} and radiative power input of 1.5 kW. This input was directly absorbed by the glass, which reached measured temperatures of 1300 °C. The temperatures predicted by the model in the melt region where the HFSS flux is initially absorbed reach maximum values exceeding 1500 °C. These conditions were maintained for 5 to 10 h and no technical problems were encountered with the containment of the hot glass melt. In all tests, the glass was completely melted notwithstanding the fact that the heat input was absorbed over an area of approximately only 20% of the total exposed melt top surface. The melt obtained from the clear glass, being more transparent, causes an overheating of the crucible bottom and inhomogeneous melting, making the process poorly controllable at this small scale. These preliminary results demonstrate that molten glass acts as an effective volumetric absorber of solar radiation up to temperatures exceeding 1300 °C.

The thermal behavior depends on the glass color due to the impact of transition ions in determining the material absorption spectrum. Ongoing work deals with the design and implementation of the heat-removal system, to further demonstrate the feasibility of the proposed TES concept.

Acknowledgements

This research has received funding from the European Union's Horizon 2020 research and innovation programme under the Marie Skłodowska-Curie grant agreement No. 656753 - GLASUNTES project. We thank Prof. R. Beerkens, M. Rongen, and M. Hubert (now at Corning Inc., US) from CelSian BV, for the insightful input over glass science and technology, J. Storck from the ETH Dept. of Earth Sciences for the support in preparing the glass samples, P. Hauterer from the ETH Institute of Energy Technology for the support with the HFSS operation, and the company Vetropack for providing the glass samples.

References

- Ades, C., Toganidis, T., Traverse, J., 1990. High temperature optical spectra of soda-lime-silica glasses and modelization in view of energetic applications. *J. Non-Cryst. Solids* 125, 272–279.
- Almath Crucibles, 2018. Material properties. Available online at <https://almath.co.uk/pages/material-properties> (Accessed June 2018).
- ANSYS (2018). ANSYS Fluent 18.2 - Theory Guide. Technical Report.
- Badenhorst, H., Fox, N., Mutalib, A., 2016. The use of graphite foams for simultaneous collection and storage of concentrated solar energy. *Carbon* 99, 17–25.
- Bamford, C.R., 1978. *Colour Generation and Control in Glass*. Elsevier Scientific Publishing Co., Amsterdam and New York.
- Bingham, P.A., Connelly, A.J., Hyatt, N.C., Hand, R.J., 2011. Corrosion of glass contact refractories for the vitrification of radioactive wastes: a review. *Int. Mater. Rev.* 56, 226–242.
- Cable, M., 2006. *Classical glass technology*. In: *Materials Science and Technology*. Wiley-VCH Verlag GmbH & Co. KGaA, Berlin.
- Cárdenas, B., León, N., Pye, J., García, H., 2016. Design and modeling of a high temperature solar thermal energy storage unit based on molten soda lime silica glass. *Sol. Energy* 126, 32–43.
- Choudhary, M.K., Potter, R.M., 2005. Heat transfer in glass-forming melts. In: Pye, L.D., Montenero, A., Joseph, I. (Eds.), *Properties of Glass-Forming Melts*. CRC Press, Boca Raton, FL - USA.
- Churchill, S.W., Chu, H.H., 1975. Correlating equations for laminar and turbulent free convection from a vertical plate. *Int. J. Heat Mass Transf.* 18, 1323–1329.
- Davis, D., Müller, F., Saw, W., Steinfeld, A., Nathan, G., 2017. Solar-driven alumina calcination for CO_2 mitigation and improved product quality. *Green Chem.* 19, 2992–3005.
- Elkin, B., Finkelstein, L., Dyer, T., Raade, J., 2013. Molten oxide glass materials for thermal energy storage. *Energy Procedia* 49, 772–779 Presented at the SolarPACES 2013 International Conference, Sept. 17–20, Las Vegas, USA.
- Endrýs, J., Geotti-Bianchini, F., De Riu, L., 1997. Study of the high-temperature spectral behavior of container glass. *Glass Sci. Technol.: Glastechnische Berichte* 70, 126–136.
- Epstein, M., Segal, A., Yogev, A., 1999. Molten salt system with a ground base-integrated solar receiver storage tank. *J. De Phys. IV: JP 9 Pr3-95 - Pr3-104*.
- Eryou, N., Glicksman, L., 1972. An experimental and analytical study of radiative and conductive heat transfer in molten glass. *J. Heat Transfer* 94, 224–230.
- Faber, A.J., 2002. Optical properties and redox state of silicate glass melts. *C. R. Chim.* 5, 705–712.

- Field, R.E., Viskanta, R., 1993. Spectral remote sensing of the dynamic temperature distribution in glass plates. *Glastechnische Berichte* 66, 118–126.
- Furler, P., Steinfeld, A., 2015. Heat transfer and fluid flow analysis of a 4 kW solar thermochemical reactor for ceria redox cycling. *Chem. Eng. Sci.* 137, 373–383.
- Gil, A., Codd, D., Zhou, L., Trumper, D., Campbell, R., Grange, B., Calvet, N., Armstrong, P., Slocum, A., 2015. Design of a 100 kW concentrated solar power on demand volumetric receiver with integral thermal energy storage prototype. In: Proceedings of the ASME 2015 Power Conference (POWER2015).
- Gil, A., Grange, B., Perez, V., Tetreault-Friend, M., Codd, D., Calvet, N., Slocum, A., 2017. CSPonD demonstrative project: Start-up process of a 25 kW prototype. In: Proceedings of the 22nd SolarPACES Conference 2016, AIP Conf. Proc. vol. 1850, paper 110003, 1–6, pp. 110003–1–110003-6.
- Glicksman, L., Renier, G., 1973. Errors associated with temperature measurements in hot glass. *J. Am. Ceram. Soc.* 56, 250–253.
- Herrera, R., Elkin, B., Raade, J., Carey, V., 2017. Modeling of flow and heat transfer in a molten glass mini-film for high temperature heat collection in a falling-film solar central receiver. *Heat Transfer Eng.* 38, 1331–1342.
- Jelley, N., Smith, T., 2015. Concentrated solar power: Recent developments and future challenges. *J. Power Energy* 229, 693–713.
- Kapyfract A.G., 2016. Thermal conductivity of Rigid materials after long exposure to high temperature. Personal communication.
- Kinzie, P., 1973. Thermocouple Temperature Measurement. John Wiley and Sons, New York.
- Kraus, D., Horst, L. (Eds.), 2002. *Mathematical Simulation in Glass Technology*. Springer-Verlag.
- Kuravi, S., Trahan, J., Goswami, D., Rahman, M., Stefanakos, E., 2013. Thermal energy storage technologies and systems for concentrating solar power plants. *Prog. Energy Combust. Sci.* 39, 285–319.
- Lee, K., Viskanta, R., 2001. Two-dimensional combined conduction and radiation heat transfer: Comparison of the discrete ordinates method and the diffusion approximation methods. *Num. Heat Transfer; Part A: Appl.* 39, 205–225.
- van Leer, B., 1979. Towards the ultimate conservative difference scheme - V. A second-order sequel to Godunov's method. *J. Comput. Phys.* 32, 101–136.
- Leibfried, U., Ortjohann, J., 1995. Convective heat loss from upward and downward-facing cavity solar receivers: measurements and calculations. *J. Sol. Energy Eng., Trans. ASME* 117, 75–84.
- Mehos, M., Turchi, C., Vidal, J., Wagner, M., Ma, Z., 2017. Concentrating Solar Power Gen3 Demonstration Roadmap. Technical Report NREL/TP-5500-67464 National Renewable Energy Laboratory, U.S. Department of Energy.
- Modest, F., 2013. *Radiative Heat Transfer*, 3rd ed. Academic Press.
- Muramoto, K., Takahashi, Y., Terakado, N., Yamazaki, Y., Suzuki, S., Fujiwara, T., 2018. VO₂-dispersed glass: A new class of phase change material. *Scientific Reports*, 8.
- Pelay, U., Luo, L., Fan, Y., Stitou, D., Rood, M., 2017. Thermal energy storage systems for concentrated solar power plants. *Renew. Sustain. Energy Rev.* 79, 82–100.
- Petrash, J., 2010. A free and open source Monte Carlo ray tracing program for concentrating solar energy research. In: Proceedings ASME 2010 4th International Conference on Energy Sustainability, pp. 125–132.
- Petrash, J., Coray, P., Meier, A., Brack, M., Häberling, P., Wuillemin, D., Steinfeld, A., 2007. A novel 50 kW 11,000 suns high-flux solar simulator based on an array of xenon arc lamps. *J. Sol. Energy Eng., Trans. ASME* 129, 405–411.
- Pilon, L., Janos, F., Kitamura, R., 2014. Effective thermal conductivity of soda-lime silicate glassmelts with different iron contents between 1100 °C and 1500 °C. *J. Am. Ceram. Soc.* 97, 442–450.
- Prieto, C., Cooper, P., Fernández, A., Cabeza, L., 2016. Review of technology: Thermochemical energy storage for concentrated solar power plants. *Renew. Sustain. Energy Rev.* 60, 909–929.
- Rabl, A., 1976. Tower reflector for solar power plant. *Sol. Energy* 18, 269–271.
- Romero, M., Steinfeld, A., 2012. Concentrating solar thermal power and thermochemical fuels. *Energy Environ. Sci.* 5, 9234–9245.
- Rosseland, S., 1936. *Atomic Theory and the Analysis of Stellar Atmospheres and Envelopes*. Clarendon Press, Oxford.
- Segal, A., Epstein, M., 1999. Reflective solar tower as an option for high temperature central receivers. *J. Phys. IV* 9 Pr3–53 – Pr3–58.
- Selkregg, K., 2018. Fusion cast refractories: Roles of containment. *Am. Ceram. Soc. Bull.* 97, 21–28.
- Seward III, T., Vascott, T., (Eds.), 2005. *High Temperature Glass Melt Property Database for Process Modeling*. The American Ceramic Society, Westerville, OH - USA.
- Slocum, A., Codd, D., Buongiorno, J., Forsberg, C., McKrell, T., Nave, J.-C., Papanicolas, C., Gobeity, A., Noone, C., Passerini, S., Rojas, F., Mitsos, A., 2011. Concentrated solar power on demand. *Sol. Energy* 85, 1519–1529.
- Steinfeld, A., 1997. High-temperature solar thermochemistry for CO₂ mitigation in the extractive metallurgical industry. *Energy* 22, 311–316.
- Stephan, K., Laesecke, A., 1985. The thermal conductivity of fluid air. *J. Phys. Chem. Ref. Data* 14, 227–234.
- Taumoefolau, T., Paitoonsurikarn, S., Hughes, G., Lovegrove, K., 2004. Experimental investigation of natural convection heat loss from a model solar concentrator cavity receiver. *J. Sol. Energy Eng., Trans. ASME* 126, 801–807.
- Touloukian, Y.S., Dewitt, D.P., 1972. Thermal radiative properties: Nonmetallic solids. In: *Thermophysical Properties of Matter*, vol. 8 IFI/Plenum Data Corp., New York.
- Viskanta, R., Anderson, E., 1975. Heat transfer in semitransparent solids. *Adv. Heat Transfer* 11, 317–441.
- Viskanta, R., Hommert, P., Groninger, G., 1975. Spectral remote sensing of temperature distribution in semitransparent solids heated by an external radiation source. *Appl. Opt.* 14, 428–437.
- Viskanta, R., Song, T.-H., 1985. On the diffusion approximation for radiation transfer in glass. *Glastechnische Berichte* 58, 80–86.
- Zhang, H., Baeyens, J., Cáceres, G., Degréve, J., Lv, Y., 2016. Thermal energy storage: Recent developments and practical aspects. *Prog. Energy Combust. Sci.* 53, 1–40.